River Flow 2010 - Dittrich, Koll, Aberle & Geisenhainer (eds) © 2010 Bundesanstalt für Wasserbau ISBN 978-3-939230-00-7

# Development of a LED-based PIV/PTV system: Characterization of the flow within a cylinder wall-array in a shallow flow

D. Groß, W. Brevis & G. H. Jirka.
*Institute for Hydromechanics, Karlsruhe Institute of Technology, Karlsruhe, Germany*

ABSTRACT: A Light Emitting Diode (LED)-based PIV system is introduced. The aim of this development is to present a flexible and cost-effective alternative to the laser-based illumination systems normally used for fluid mechanics and hydraulics measurements. Industrial cameras, a computer with raid, software for acquisition and control, a fully programmable digital sequencer and an array of high-power LEDs, compose the system. The LEDs can be used as a continuous or as a pulsed light source, and in the latter case can be fully synchronized with a mono or multi-camera system. This enables, in addition to PIV and PTV, the realtime vectorization of flow fields by particle tracing. A demonstration of the system capabilities is presented, when the flow structure within an array of emerged cylinders is investigated. The LED light source was able to illuminate the whole horizontal measurement area, avoiding the generation of shadows, normally induced by the cylinder array when a single light source is used. The results show a predominant diagonal movement towards the main channel, and almost no difference between the parameters analyzed at two water depths, an indication of a potentially two-dimensional flow structure.

*Keywords: PIV, PTV, LED, Shallow flow, Vegetated flow.*

## 1 INTRODUCTION

Image Velocimetry has become a standard technique for velocity measurements in fluid mechanics and Hydraulics. The idea is to seed the flow with a tracer, particles or phosphorescent dye, and to record its movements by one or more cameras. Once the position of the tracer is detected in two sequential images, or a single double exposure image, the displacements at different spatial locations are calculated (Adrian, 2005). Using the time between frames the velocity field can be determined. Depending on the technique used for the determination of the velocity field, Image Velocimetry can be mainly classified in Particle Image Velocimetry (PIV), Particle Tracking Velocimetry (PTV) or Molecular Tagging Velocimetry (MTV). The first one uses a Eulerian frame of reference, and allows the determination of two-dimensional (2D) or three-dimensional (3D) velocity fields based on the displacement of groups of tracers. The second one uses a Lagrangian frame and allows also the determination of a 2D or 3D velocity field, but based on the determination of the displacements of individual tracers. The same principle of PIV is used by MTV, but instead of particles, uses a pattern of phosphorescent dye tagged by a laser light (Gendrich, 1997).

From a technical point of view, one common characteristic of these techniques is the use of expensive instrumentation to illuminate and record the tracer motion. Normally, a system designed to accomplish these measurement consists of a light-source and optics (normally laser and cylindrical lens), a mono or multi-camera system, a sequencer for synchronization, and a storage system. The use of a laser as illumination, involves many advantages, but also operative disadvantages. One of the disadvantages is their high price, the necessary safety-measurements surrounding their operation, and the difficulties involved when they are used in field measurements.

In this paper the development and application of a Light Emitting Diode (LED) PIV/PTV system at the Institute for Hydromechanics, Karlsruhe Institute of Technology (KIT) is presented. The main objective of this project is to introduce a flexible and cost-effective alternative to the laser-based illumination systems normally used in fluid mechanics and hydraulics. Firstly, a detailed de-

scription of its components, and a discussion of their associated technical restrictions, is presented. Secondly, a demonstration of the system capabilities is presented. For this, the flow structure within a cylinder array attached to a channel-side is measured at two horizontal positions. The paper finalizes with some recommendations, and a discussion of future applications for LED based systems.

## 2 LED ILLUMINATION DESCRIPTION

In order to produce a proper light source, instead of the ND-YAG-Pulse-Lasers commonly used for illumination in PIT/PTV, an array of Light Emitting Diodes was built. Each array basically consists of several high-power LEDs, current-controllers and a cylindrical lens, used to parallelize the light in its central zone. The LEDs are aligned in a row and mounted on an aluminum square pipe. The pipe is internally filled by flowing water and acts as the mechanical framework of the whole construction and as the heat-sink/chiller for the LEDs and the current controllers (See Figure 1 and 2).

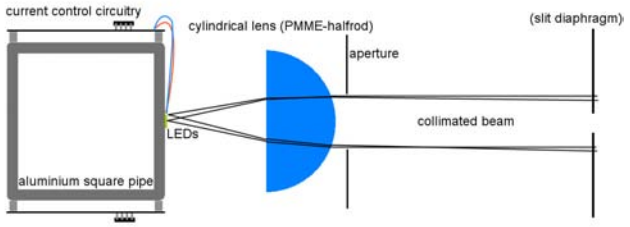


Figure 1 Schematic composition of an LED-array

The peak of the emission spectrum of the LEDs is at 470 nm, and their spectral half-width, which is the spectral width at 50 % of its peak intensity, is 33 nm. This wavelength was chosen as it proved to match the spectral range of the peak sensitivity of the selected cameras and additionally, is the range where the LEDs of the selected manufacturer have their highest efficiency.

Compared to Lasers the LEDs have comparative advantages in the following areas:

*Safety*: The advantage in terms of safety results from the fact that the light generated by an LED-array is never concentrated into a thin ray as it is with a Laser, instead a sheet of light is generated from the source, resulting in a small peak-power density.

*Divergence of the lightsheet*: In order to obtain a narrow lightsheet a slit diaphragm is placed at the required starting point of the lightsheet. The distance from the LED-array to the diaphragm and the width of the diaphragm-aperture are the main factors determining the divergence of the lightsheet. For larger distance, between lens and object, and narrower diaphragm -aperture the light divergence is smaller, however the luminous density decreases. In the experiments described in this paper, over a distance of 0.7 m, the plane widened from 3 mm, opening of the slit diaphragm, to 8 mm, i.e. a divergence of the lightsheet of 7 mrad. While this value is high compared with Lasers, typical values are 0.5 mrad for gaussian resonators and 4 mrad for stable resonators, the width of the non-intrusive light plane is still smaller in this case than the sample volume of common ADV-sensors (Acoustic Doppler Velocimetry).

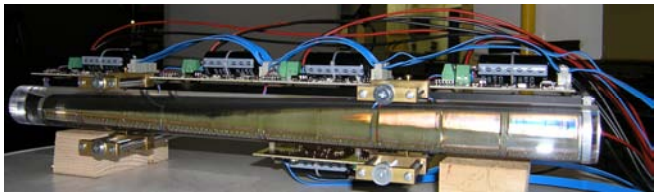

Figure 2 Electronic and optic of the LED-array.

*Volumetric illumination:* When used for volumetric illumination as needed for three dimensional measurements (Pereira et al, 2006), the whole radiometric flux of the LED-arrays, which is more than 200W of light at 2,7KW electrical input, is used, resulting in high luminous density in the volume of measurement.

*Flexibility*: Handling the LED-arrays is generally easier than handling a Laser as their weight is low and they are much more shock-resistant. Another advantage is the fact that no protections against reflecting rays of light are necessary. Thus modifications on the PIV/PTV-setup are done in a fraction of the time.

*Economy*: Currently it is not possible to give reliable information on what the retail price of industrially manufactured systems would be, but it is very likely that it will be a fraction of a Lasers price.

### 2.1 *PIV/PTV system*

In this section a brief description of the components of the PIV/PTV system is presented. Several modes of operation of the system are possible, and they are defined using a software developed to configure a digital sequencer that is used to synchronize the operation of the components. The signals emitted by the sequencer are received by the mono/multi camera equipment and by the LED array. The pictures are streamed back to the computer and stored in a built-in RAID system. An overview of the system is presented in Figure 3.

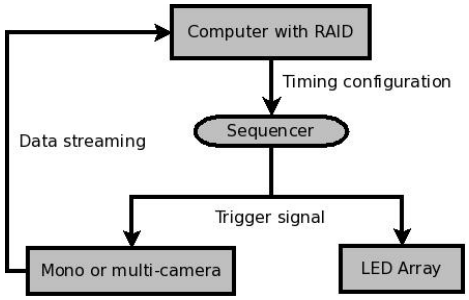

Figure 3 Schematic representation of the PIV/PTV system.

### 2.1.1 *Cameras*

The system uses two industrial grade cameras for image acquisition. While the manufacturer of the cameras offers a variety of models with different resolutions and maximum frame rates, the ones chosen for the system described here feature a one-inch CCD-sensor with 1600x1200 pixel (2 MP) and a greyscale-resolution of 8 or 12 bit. The sensor has a pixel size of 7,4² µm² and a quantum efficiency of 55 % at 470 nm.

The cameras connect to a PC via the standardized Gigabit Ethernet Interface and deliver a sustained frame rate of 32 frames per second (FPS), at full format, and 54 FPS at VGA resolution. Sustained means, that the duration of a continuous recording is only limited by the size of the data storage (~6 hours for the current system using a single camera).

### 2.1.2 *Sequencer and synchronization*

A sequencer generally is found in PIV-Systems and is needed for precise and uniform (with regards to timing) acquisition of the images and synchronous operation of the device used for illumination (usually a Laser). Additionally, the acquisition of data from further sensors (e.g. pressure) may be synchronized to the acquisition of the images in order to have a common time base and thus to be able to relate measured phenomena. The sequencer we developed is based on a FPGA (Field Programmable Gate Array, a programmable logic-chip). Up to eight signals can be configured in three different modes of operation: It is possible to have a signal running independently at a specific frequency, to have it reacting once to another signal with a certain delay and to have it running while another signal is in a certain state. Additionally it is possible to combine signals with binary logic. This flexibility in configuring the signals allows using the sequencer for a wide variety of tasks. Not only the different modes of operation of the LED-based PIV-System can be controlled but also all Laser based systems in single-, double-frame and autocorrelation mode. Even curious things like alternating image acquisition on two or more cameras are possible and the configuration is done in a minute once the principle logic is understood. The sequencer has a timing resolution of 20 ns. Its electrical outputs can drive loads of up to 50 mA at 5 V, ensuring low signal-lag even when using long cables. Optionally they can be switched to operate at 12 V for greater flexibility.

### 2.1.3 *Software*

For the chosen cameras there was no software available that allowed for the continuous acquisition and storage of images. Due to this a software was developed for this purpose.

The software is written in c++ and features a multithreaded architecture. The primary design goals, besides stability and reliability, which are obligatory, were low CPU-usage, a high responsiveness and a high performance disc-IO.

The software is currently designed to operate with one or two cameras. It features a zoomable realtime preview (live-view) for both cameras that requires little CPU-time. Due to its multithreaded architecture and low CPU-usage, the live-view has no influence on the process of recording images and can stay active during the experiment. This is especially useful for the observation of extended experiments where the probability of errors (e.g. running out of seeding) is higher.

The ability to record a series of images from two cameras synchronously was of particular importance. In order to guarantee that a pair of images (frames) acquired from the two cameras really belongs to the same point in time, the software checks the timestamp of each frame, and automatically re-synchronizes the two image-streams in case that an image was lost.

### 2.1.4 *Computer / Storage System*

A single computer controls the whole system. This computer, based on a common quad-core CPU (X86 compatible) running at 2,83 GHz, contains a RAID-array of harddisks with a total capacity of 1.2 TB expandable up to 4 TB. In the experiments presented here the computer was used to record the images streamed by two 2 MP cameras working at full resolution and 32 FPS. The RAID-array built in the current system allowed the recording of up to ~3 hours with the selected camera configuration.

## 2.2 *Modes of operation*

The system can be operated in four different modes. The current controllers enable these different modes of operation. The electrical current driven through the LEDs, $I_D$, determines their radiometric output power, the relation is roughly linear. Simply put : the higher the current, the higher the light-intensity. The current controllers are responsible for regulating $I_D$ and thus the brightness of the LEDs. Depending on the mode of operation, different temporal patterns of illumination are required. By means of the digital sequencer, that connects to the current controllers, $I_D$ can be switched between three possible values: off (zero), value1 and value2, where value1 and 2 can be preselected in the range of 0 to 5000 mA. The current controllers are precise and fast; the time it takes to switch to a new value is well below 1 µs. Due to their rapidness it is possible to precisely generate the illumination-patterns required for each mode of operation.

The current controllers also allow for overdriving the LEDs for short periods of time. That is, driving more current through the LEDs than permitted for continuous operation (i.e. more than 1000 mA). This characteristic is useful for stroboscopic illumination where short illumination times are required. Overdriving is possible because the primary factor limiting $I_D$ is the temperature of the LED-die (the "die" is the "chip" inside the LED that actually generates the light). If the duration of the pulses is kept short enough, the LED-die will not heat above the maximum permitted temperature.

To protect the LEDs against incorrect operation, there is an overload protection implemented in the current-controllers, to limit the pulse-duration when overdriving the LEDs. The overload protection limits the integral of current over time to about 3 mAs and thus ensures a safe operation.

The last feature of the current controllers is to provide feedback to the user regarding the measurement of the real $I_D$ when operating the LEDs in a pulsed fashion. Two analogue sample and hold stages measure $I_D$ during the duty-cycle of the pulses when value1 respectively value2 is desired and transform the amplitude of the pulses into a continuous signal. This enables to check the currents at which the LEDs operate without having to use an oscilloscope.

### 2.2.1 *Cross-correlation-mode*

When performing PTV/PIV based on cross-correlation, the displacement of the particles (PTV) or a group of particles (PIV) is determined by comparing two subsequent images at a time (Westerweel, 1997). Thus the LEDs need to emit a single flash of light for each frame. The duration of the flash must be short and accordingly, the power of the LEDs (respectively $I_D$) high in order to keep motion-blur low. The timing-diagram shown in Figure 4 illustrates this mode where the LEDs operate in a pulsed fashion synchronous to the camera(s).

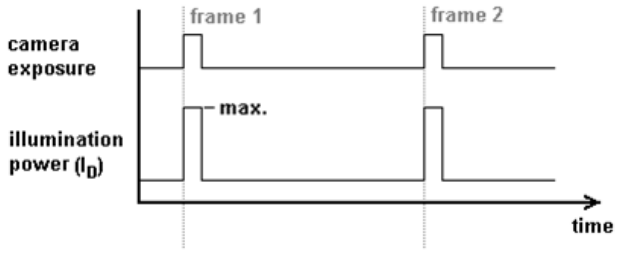


Figure 4 Timing diagram for the acquisition of images to be analyzed by cross-correlation

An example obtained by this illumination-pattern is shown in Figure 5. The image simply shows a snap-shot of the particles.

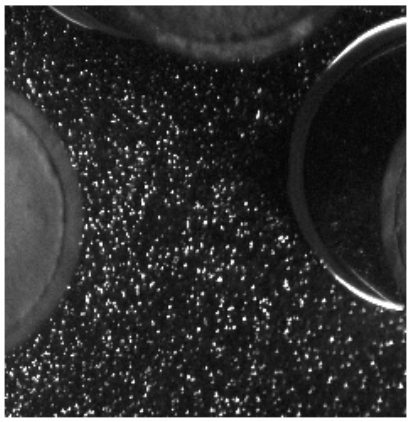

Figure 5 Example image for cross-correlation. Shown is a section of 238x244 pixel out of a 1600x1200 pixel image

### 2.2.2 *Auto-correlation-mode*

In contrast to cross-correlation, when auto-correlation is used, the displacement of the particles or a group of particles is determined within a single image (Adrian, 1991). Accordingly the particles need to be illuminated twice in each image (double-exposure). Again, short illumination-times are desired. Figure 6 shows the corresponding timing-diagram. The images obtained by this illumination-pattern show snap-shots of the particles where each particle is pictured twice (Figure 7).

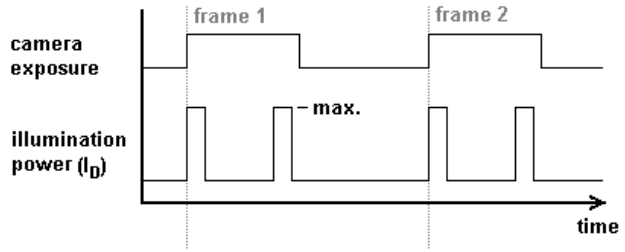

Figure 6 Timing diagram for the acquisition of images to be analyzed by auto-correlation


Figure 7 Example image for auto-correlation

### 2.2.3 *Particle tracing-mode*

Acquiring an image with a long exposure time where $I_D$ is low and then maximizing $I_D$ right before the end of the exposure yields a picture where the traces of the particles are visible and a brighter dot marks end of each trace, thus making the whole flow field -including directional information- instantly visible The timing diagram is shown in Figure 8, a resulting image is shown in Figure 9.

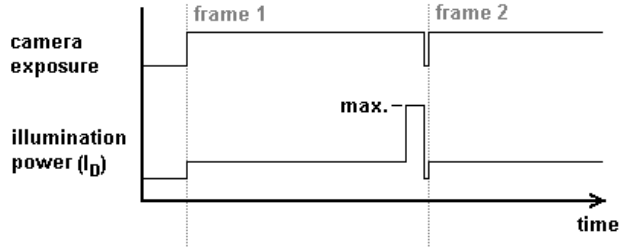

Figure 8 Timing diagram for the acquisition of images in particle tracing-mode

Particle tracing provides two advantages and complements perfectly with PIV/PTV. First, it shows the flow structures with a unbeaten density of information and second, the information is available immediately, no computing-intensive processing is required. It is an excellent tool for visualization and for checking/verifying the plausibility of the results obtained by PIV/PTV as it reveals the structures that were missed or filtered out by the PIV/PTV- and post-processing-algorithms. Currently it is rarely used, as it was hard to accomplish with the devices traditionally used for illumination (Ruck, 1996).


Figure 9 example of particle tracing mode

### 2.2.4 *Continuous illumination-mode*

The fourth mode is simply continuous illumination. Continuous illumination will in most cases not be used for any actual measurement. Instead it is useful for setting the PIV/PTV-system, e.g. for the adjustment of the lightsheet or for viewing the fluid flow by eye as it avoids the disturbing flickering involved with the pulsed operation of the LEDs.

Of course the operation of the LEDs is not limited to the four modes presented here. Instead, with a suitable sequencer, any arbitrary pattern can be generated by switching between the three possible states $I_D$=0, value1 or value2.

## 3 FLOW WITHIN A CYLINDER WALL-ARRAY IN A SHALLOW FLOW.

To demonstrate the capabilities of the system, the flow within an array of cylinder in a shallow flow was measured. The experiments were conducted in a 17 m long and B = 1.8 m wide, rectangular tilting flume at the Institute for Hydromechanics, Karlsruhe Institute of Technology. The longitudinal slope for the experiments was fixed to approximately S=0.001. The flume bottom consisted of laminate plastic with small sand elements of diameter less than 0.002 m. The flume inflow was connected to a constant head tank and the flow rate controlled by an inductive flow meter together with a computer-controlled gate valve. In order to avoid the formation of upstream perturbations, the flow was aligned by using a honeycomb diffuser of about 0.2 m wide. The cylinder array was modeled by placing single cylinders of d=6.3 cm of diameter. The array had a total width, W= 37.8 cm and length L=44.1 cm, and it was placed at one side of the flume. The discharge was constant and equal to 0.01 m³/s, with a uniform water depth

in the measurement area of H=4 cm and a cross-sectional bulk velocity of about V=0.14 m/s. A general view of the experimental geometry is presented in Figure 10. This geometry was selected due to the complexity associated to similar experiment when a single laser is used. In such cases, the flow within the array is partially covered by shadows induced by the cylinders. A similar situation can appear if one LED array is used, however the illumination system is modular, and can be divided in individual arrays of 100 LEDs. In order to avoid the shadow formation, 2 of these LEDs modules were located in such a way that the light direction was able to enter in the cylinder array without shadow formation (see Figure 10).

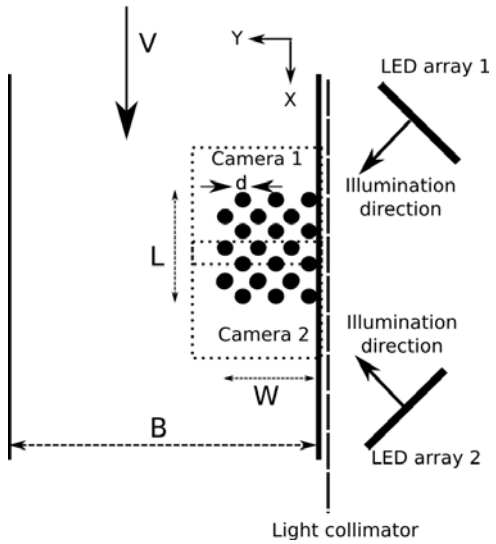


Figure 10 Schematic representation of the experimental setup.

The flow was seeded with polyamide particles of 100 μm mean diameter ($d_{50}$). Two synchronized cameras were vertically positioned to record the particle motion, each one covering about half of the cylinder array (see Figure 9). The cameras were operated at full resolution, 2 MP, with an acquisition frequency of 32 Hz. Two horizontal planes were measured, each for 5 min, i.e. a total of 9600 images frames were acquired per measurement position. The acquired images were analyzed using the GNU Particle Image Velocimetry software GPIV (Van der Graaf, 2010). A multi-pass image deformation algorithm was used, where the final interrogation window had a size of 32x32 pix. This interrogation window contained, a mean value higher than 15 particles.

The resulting velocity fields were filtered using an iterative Matlab-implementation of the normalized median filter proposed by Westerweel and Scarano (2005), using an acceptable fluctuation of the velocity due to cross-correlation of 0.3 and threshold for the normalized residuals of 3.

The horizontal measurement planes were located at h=2 cm and h=3 cm, i.e. h/H=0.5 and h/H=0.75, respectively.

Flow visualizations showed that most of the flow within the cylinder array was deflected towards the main channel and that the velocity flow downstream the array was significantly reduced.

Similar to the results presented by Zima & Ackermann (2002), and Naudascher & Rockwell (1994), a strong water surface oscillation induced by the vortex shedding phenomena generated by the cylinder array was observed.

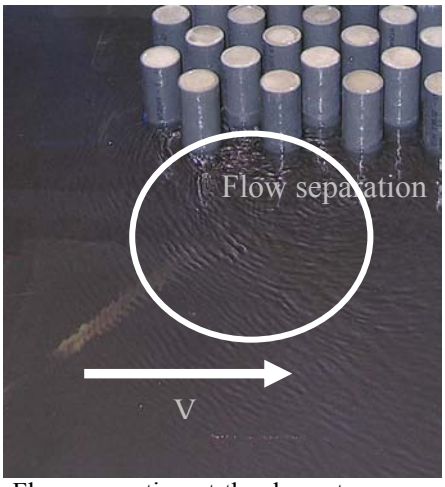


Figure 11 Flow separation at the downstream corner of the cylinder array.

### 3.1 *Mean velocity field*

In Figure 12, the mean, two-dimensional, velocity field, $\sqrt{u(x)^2 + v(y)^2}$ for H/h=0.5 is shown. As observed in the flow visualization, the mean flow was characterized by a strong deflection of the upstream flow towards the main channel. All diagonal channels, formed between cylinders, shown a predominant flow towards the main-channel, and due to this, several local cylinder-wakes are also showing a diagonal structure (see the mean vorticity field shown in Figure 13). The comparison of the results between different depths, showed almost no difference, which is evidence that the mean flow structure within the array was essentially two-dimensional. However a detailed analysis of the image series showed an important vertical motion in the intersection of the diagonal channels (see Figure 14). Due to the flow separation, the velocity at the upstream–main channel corner of the cylinder array was increased about a 40 % respect to V, while the maximum velocity in the dominant diagonal channels, downstream the third row of cylinder, was approximately 40 % less than V. The larger coherent structures observed, were generated by vortex shedding at the downstream cylinder located at

(X=37.8,Y=25.2), their characteristic length scale was of the order of d.

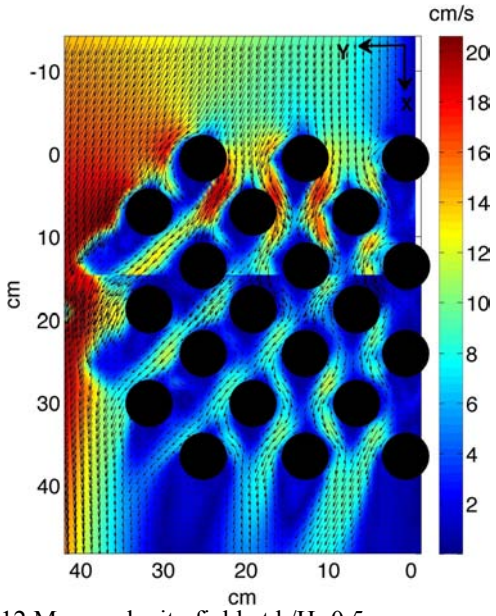


Figure 12 Mean velocity field at h/H=0.5

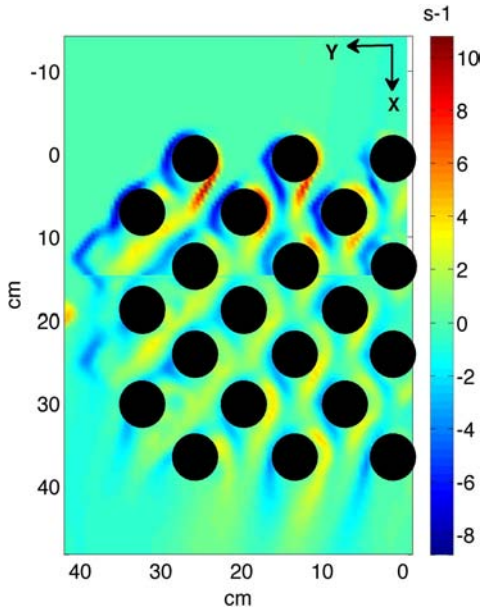


Figure 13 Mean vorticity field at h/H=0.5

## 3.2 *Reynolds Stress*

In figure 15, the cross-correlation between velocity fluctuation in x and y direction, $u(x,t)'v(x,t)'$ is presented. Even thought most of the random activity was observed, based on the flow visualizations, at the channel intersection, the results reveal that most of the momentum fluxes occur at the channels itself, with negative magnitudes in the dominant channels, i.e. those with flow from the wall towards the main channel, and positive magnitude in those with opposite flow direction.

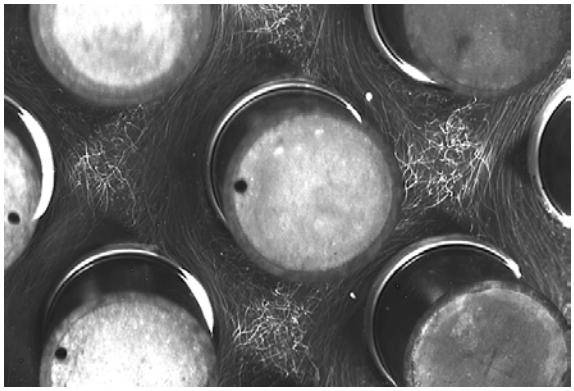

Figure 14 long-exposure images showing the complex flow at the channel intersections. The flow is visualized by glowing traces drawn by the particles

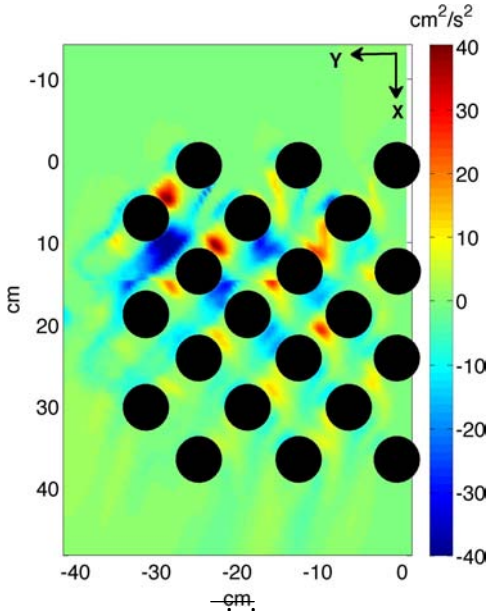


Figure 15 Reynolds stress $\overline{u'v'}$ at h/H=0.5

## 3.3 *Pseudo – Turbulent Kinetic Energy*

The pseudo turbulent kinetic energy $\overline{u'^2}+\overline{v'^2}$ is presented in Figure 16. As expected, the higher levels of kinetic energy are located in the diagonal channels, where the mean velocity is directed towards the main channel. A comparison of this information and the Reynolds stress shown in Figure 15, clearly indicate that most of the turbulent activity occurs in the region contained in the first four rows, from upstream to downstream direction, and that the energy dissipation of the freestream flow must occur mainly in that region. Similar to the mean velocity field, both, Reynolds stress and pseudo kinetic energy present almost no variation when the two measured planes were compared.

Of course, the region where most turbulent activity occurs is a function of the geometry and porosity; as a consequence these preliminary results must be taken only as particular ones.

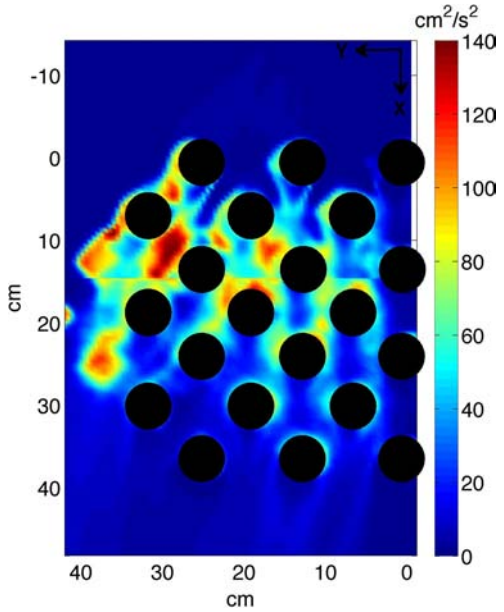

Figure 16 Pseudo Turbulent Kinetic Energy (TKE) at h/H=0.5

## 4 OTHER APPLICATIONS

Due to the portability, shock resistance, and low cost, one of the natural applications of the LED system are field measurements in shallow water bodies. Another application is the design, not only of a LED line, but its extension to a full matrix, that can be used to scan a volume and to perform quasi-three dimensional PIV/PTV measurements.

All these applications can also involve the visualization of a fluorescent tracer such as Fluorescein, which has an absorption maximum at 494 nm, very close to the 470 nm emitted by the LED array presented here. The homogeneity of the light source makes its use particularly adequate for concentration measurements in small regions, where the natural divergence of the light could be neglected.

Finally, it is necessary to point out that any divergence existing in the light source is not longer important if multi-camera, three-dimensional measurements are involved. In these cases the processing of the information allows the recovering of the cross-plane position of the calculated velocities. In this situation the error induced by the light divergence is complete avoided.

## 5 CONCLUSIONS

In this work a novel LED based PIV/PTV system was presented. Based on the preliminary tests, and on the measurements presented here, it is possible to point out that this system is a real, cost effective alternative to traditional Laser-based systems. It is expected that further works on the development of this system will provide a flexible tool not only for laboratory, but also for field measurements.

The experimental results provided here show that even though a complex flow structure was observed in some flow-channel intersections, the structure at different horizontal positions remained almost unchanged. Based on the latter observation it is possible to state that most of the flow structure was essentially two-dimensional. The mean turbulent statistics presented here indicate that the momentum fluxes mainly occur in the internal flow-channels, and that most of the turbulent activity is localized within the four first upstream cylinder–rows.

## ACKNOWLEDGEMENTS

The authors gratefully acknowledge the support provided by the German Science Foundation (Deutsche Forschungsgemeinschaft, DFG), Grant JI 18/18-1.

## REFERENCES

R. J. Adrian, "Particle Imaging Methods for Experimental Fluid Mechanics" in Annual Reviews of Fluid Mechanics, 1991, pp. 261-304 .

Adrian, R.J., (2005). Twenty years of particle image velocimetry. Experiments in Fluids, 39(2), 159-169.

Gendrich, C.P, Koochesfahani, M.N. & Nocera, D.G. (1997). Molecular tagging velocimetry and other novel applications of a new phosphorescent supramolecule. Experiments in Fluids, vol. 23 (5) pp. 361-372.

Naudascher, E., and Rockwell, D. 1994. Flow induced vibrations—an engineering guide, A. A. Balkema, Rotterdam, The Netherlands.

Pereira, F., Stuer, H., Graff, E. & Gharib, M. (2006). Two-frame 3D particle tracking. Measurement Science and Technology. Vol. 17(7), pp 1680-1692.

Ruck, B., 1996: “A New Flow Measuring Technique for Velocity Vector Display”, Proc. of the Int. Seminar on Optical Methods and Data Processing in Heat and Fluid Flow, City University, London.

Van der Graaf, G. (2010) "Gpiv: An open Source project for PIV". http://gpiv.sourceforge.net.

J. Westerweel “Fundamentals of digital particle image velocimetry” Meas. Sci. Technol. 8 (1997) 1379-1392.

Westerweel, J. & Scarano, F. (2005). Universal outlier detection for PIV data. Experiments in Fluids . Vol 39(6), pp 1096-1100.

Zima, L. and Ackermann, N. (2002). Wave Generation in Open Channels by Vortex Shedding from Channel Obstructions. J. Hydr. Engrg. Volume 128, Issue 6, pp. 596-603